Journal of Molecular Structure 1196 (2019) 805–818

Contents lists available at ScienceDirect

Journal of Molecular Structure

journal homepage: http://www.elsevier.com/locate/molstruc

Synthesis, spectroscopic studies, DFT calculations, antimicrobial and antitumor activity of tridentate NNO Schiff base metal complexes based on 5-acetyl-4-hydroxy-2*H*-1,3-thiazine-2,6(3*H*)-dione

Omima M.I. Adly*, Hoda F. El-Shafiy, Magdy Shebl

Department of Chemistry, Faculty of Education, Ain Shams University, Roxy, Cairo, 11711, Egypt

ARTICLE INFO

Article history:
Received 22 May 2019
Received in revised form
27 June 2019
Accepted 2 July 2019
Available online 3 July 2019

Keywords:
Tridentate schiff base
5-Acetyl-4-hydroxy-2H-1,3-thiazine-2,6(3H)-dione
DFT
Thermal analysis
Antimicrobial activity

ABSTRACT

New Schiff base ligand was prepared by condensation of 5-acetyl-4-hydroxy-2*H*-1,3-thiazine-2,6(3*H*)-dione with *o*-phenylenediamine. Cu(II), Ni(II), Co(II), VO(IV), Zn(II), Cd(II) and UO_2(VI) complexes were prepared and characterized on the basis of elemental analyses, IR, (^{1}H and ^{13}C) NMR, electronic, ESR and mass spectra; magnetic, molar conductance measurements as well as thermal gravimetric analysis. The coordination sites of the Schiff base ligand are phenolic oxygen, azomethine nitrogen and amino group nitrogen; where the ligand acts as monobasic tridentate. All results established that all compounds have 1:1 (metal: ligand) stoichiometry except Ni(II)- and VO(IV)- complexes have 1:2 (metal: ligand) stoichiometry. The metal complexes showed octahedral geometry except Cu(II) complex which showed square planar arrangement and UO_2(VI) has pentagonal bipyramidal arrangement. Thermodynamic parameters were calculated for the ligand and its metal complexes using Coats-Redfern method. The ligand and its complexes were tested *in vitro* bioassays against some Gram-negative and Gram-positive bacteria and the fungus strain; showing good results for some of these compounds. The antitumor activity of the ligand and its copper(II) and oxovanadium(IV) complexes was investigated against HepG2 cell line. Density Function Theory (DFT) level implemented in the Gaussian 09 program was used to optimize structure and some structural parameters of the ligand and its metal complexes such as: total energy, HOMO, LUMO as well as dipole moment. The computed data were correlated with the experimental results.

1. Introduction

Schiff bases represent one of the most important chelating ligands in coordination chemistry [1,2]. They are utilized as catalysts [3], dyes and pigments, intermediates in organic synthesis and as polymer stabilizers [4]. Recently, Schiff bases have attracted a great significance due to their wide applications including photophysical [5], photoluminescence [6], thermal [7] and optical properties [8,9], as well as various biological importance [10–14]. Metal complexes of the Schiff bases have attracted a great interest because of their widespread applications including antimicrobial [15], anticancer [16], antitumor [17], antioxidant [18], anti-inflammatory [19], antiviral [20] and herbicidal [21] activities, in addition to catalytic [22], thermal [23] and electrochemical [24] properties. Compounds containing 1,3-thiazine ring attracted attention because of their antimicrobial [25], antimicobacterial [26], anticancer [27] and antitumor [28] activities.

In our previous studies [29–34], metal complexes of Schiff base ligands derived from 5-acetyl-4-hydroxy-2*H*-1,3-thiazine-2,6(3*H*)-dione (AHTD) have been fully characterized. Therefore, the present work aims to synthesize of a new Schiff base ligand (HL), by the condensation of AHTD with *o*-phenylenediamine, and its complexes with Cu(II), Ni(II), Co(II), VO(IV), Zn(II), Cd(II) and UO_2(VI) ions. The structures of the ligand and its metal complexes were characterized by elemental analyses, spectral, magnetic, molar conductance and thermal gravimetric analysis.

The ligand and its metal complexes were subjected to antimicrobial assays against selected kinds of bacteria and fungi. The antitumor activity of the ligand and its Cu(II) and VO(IV) complexes was investigated against HepG2 cell line. The theoretical data of the DFT calculations were correlated with the experimental results of the ligand and its metal complexes by means of a density functional

* Corresponding author. Tel.: +20 1008693220.
E-mail address: omima_adly@yahoo.com (O.M.I. Adly).

https://doi.org/10.1016/j.molstruc.2019.07.010
0022-2860/

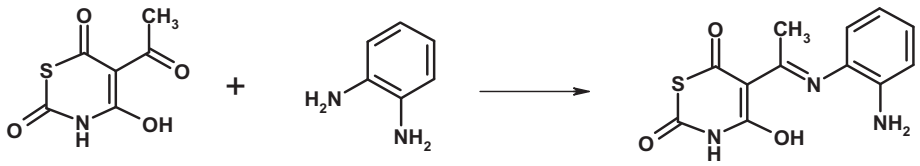

Scheme 1. Formation of the Schiff base, HL, ligand.

theory (DFT) at the B3LYP/6-311G (d,p) level using Gaussian 09 program.

2. Experimental

2.1. Materials

All employed chemicals were of reagent grade. Nitrate salts of copper(II), nickel(II), cobalt(II), zinc(II) and cadmium(II), Oxovanadium(IV) sulfate, dioxouranium(VI) acetate dihydrate were used. *o*-Phenylendiamine were BDH. Organic solvents were reagent grade. The antibiotic Doxymycin and Fluconazole were purchased from Egyptian markets and used as references for antibacterial and antifungal activities.

2.2. Synthesis of 4-hydroxy-5-[N-(2-hydroxyphenyl)ethanimidoyl]-2H-1,3-thiazine- 2,6(3H)-dione, HL, ligand

5-Acetyl-4-hydroxy-2*H*-1,3-thiazine-2,6(3*H*)-dione (AHTD) was prepared as described elsewhere [35]. Then, a mixture of 1.87 g (10.0 mmol) AHTD and 1.08 g (10.0 mmol) *o*-phenylenediamine, in (30 mL) absolute ethanol containing few drops of acetic acid, was heated under reflux for 3 h. Yellow crystals were obtained after cooling at room temperature. The product was filtered off and recrystallized from ethanol, yield 2.00 g (72%) and m.p. 194 °C. Scheme 1 illustrates the formation of the HL ligand.

2.3. Synthesis of the metal complexes

0.83 g (3 mmol) of the Schiff base ligand, in 30 mL methanol was added drop-wise to a 3 mmol of the respective metal salt in 20 mL methanol in the molar ratio 1:1. The reaction mixture of the ligand with metal salts was heated under reflux for 3 h, and then left overnight at room temperature. The precipitates were filtrated and washed with 50% (v/v) methanol-water then diethyl ether and stored in desicator.

2.4. Computational method

DFT calculations were performed on the ligand and its complexes using Gaussian 09 program package [36]. Gauss View 5.0 package was used to obtain various graphic views of molecular charges and shapes of distinctive molecular orbitals.

2.5. Antimicrobial activity

The Schiff base ligand (HL) and its metal complexes were screened for their antibacterial and antifungal, using standardized disc agar diffusion method [37,38], against the sensitive organisms *Staphylococcus aureus* as Gram positive bacteria, *Proteus vulgaris* as Gram negative bacteria and *Candida albicans* as fungus strain. The compounds were dissolved in DMSO which has no inhibition activity to get concentration of 100 μg mL^{-1}.

2.6. Antitumor activity

The antitumor activity of the Schiff base ligand (HL) and its Cu(II)- and VO(IV) complexes was carried out against HepG2 cells by determining the effect of the test samples on cell morphology and cell viability according to literature technique [39,40].

2.7. Measurements

Elemental analyses were carried out using Vario-Elementar at the Ministry of Defense, Chemical War Department. Analyses of the metal ions were carried out complexometrically [41,42]. The FT-IR spectra (4000-400 cm^{-1}) of the ligand and its complexes were recorded as KBr discs using FT-IR-4000 (Shimadzu) spectrophotometer. ^{1}H NMR (300 MHz) and ^{13}C NMR (75 MHz) spectra were recorded using a Mercury-300BB. Dimethylsulphoxide, DMSO-d_6, was used as a solvent and tetramethylsilane (TMS) as an internal reference. The electronic spectra of the ligand and its metal complexes were measured on a JASCO model V-550 UV-VIS spectrophotometer in the range 200–900 nm. ESR spectra were recorded on the Bruker, Model: EMX, X-band spectrometer. Mass spectra were obtained using GC-2010 Shimadzu Gas chromatography

Table 1
Physical and analytical data of the HL ligand and its metal complexes.

	Ligand/complex	Molecular formula	M.Wt. Yield (%)	Color	M.P.°C	Elemental Analyses sFound (calcd.) %				
						C	H	N	S	M
	HL	$C_{12}H_{11}N_3O_3S$	277.30 (72)	Yellow	194	51.96 (51.98)	4.25 (4.00)	15.20 (15.15)	11.60 (11.56)	____
(**1**)	$[CuL(H_2O)]NO_3.0.5H_2O$	$C_{12}H_{13}N_4O_{7.5}$ S Cu	428.90 (64)	Green	>300	33.15 (33.61)	3.09 (3.05)	13.12 (13.06)	7.94 (7.48)	14.63 (14.81)
(**2**)	$[Ni(L)_2].2H_2O$	$C_{24}H_{24}N_6O_8S_2Ni$	647.33 (66)	Gray	>300	44.46 (44.53)	3.21 (3.74)	12.72 (12.98)	10.40 (9.91)	9.15 (9.07)
(**3**)	$[CoL(H_2O)_3]NO_3.1.5CH_3OH$	$C_{13.5}H_{22}N_4O_{10.5}SCo$	499.34 (59)	Dark brown	>300	32.87 (32.47)	4.00 (4.44)	11.72 (11.22)	6.01 (6.42)	(11.62) (11.80)
(**4**)	$[VO(L)_2].3H_2O$	$C_{24}H_{26}N_6O_{10}S_2V$	673.50 (62)	Green	>300	42.73 (42.76)	3.34 (3.86)	12.68 (12.47)	9.61 (9.50)	NA (7.56)
(**5**)	$[Zn(L)(H_2O)_2NO_3].H_2O$	$C_{12}H_{16}N_4O_9SZn$	457.34 (58)	Yellow	>300	30.89 (31.51)	3.59 (3.52)	12.63 (12.25)	6.77 (7.01)	14.38 (14.21)
(**6**)	$[CdL(CH_3OH)_2\ NO_3]$	$C_{14}H_{18}N_4O_8SCd$	514.60 (56)	Yellow	>300	31.42 (32.67)	3.42 (3.53)	10.26 (10.88)	6.09 (6.22)	21.52 (21.76)
(**7**)	$[UO_2L(H_2O)(OAc)].\ H_2O$	$C_{14}H_{19}N_3O_{10}SU$	659.30 (43)	orange	>300	25.54 (25.48)	2.79 (2.88)	6.17 (6.37)	4.56 (4.85)	NA (36.10)

NA: not analyzed.

Table 2
Characteristic FT-IR bands (cm^{-1}) of the HL ligand and its metal complexes.

	Ligand/complex	ν(OH, NH)	ν(NH,NH_2)	ν(C=O)	ν(C=N)	ν(C=C)	ν(M – N)	ν(M – O)	Other band
	HL	3463	3388, 3315, 3222	1661	1622	1544	____	____	____
(**1**)	[CuL(H_2O)]NO_3.0.5H_2O	3431, 3184	3237, 3185	1625	1524	____	560	468	1390, 820 ν NO_3 (ionic)
(**2**)	[Ni($L)_2$].2H_2O	3464,	3351, 3278 3133	1665	1588	1534	553	439	____
(**3**)	[CoL($H_2O)_3$]NO_3.1.5CH_3OH	3422	____	1630	1565	____	545	446	1383, 829 ν NO_3 (ionic)
(**4**)	[VO($L)_2$].3H_2O	3442	3234, 3180	1625	1525	____	540	426	1095ν (V=O)
(**5**)	[Zn(L)($H_2O)_2NO_3$].H_2O	3425	3367	1625	1553	1510	507	473	(1350,1216) νNO_3 (unidentate)
(**6**)	[CdL($CH_3OH)_2$ NO_3]	3455	3388, 3257	1630	1545	1448	550	438	(1356,1230) νNO_3 (unidentate)
(**7**)	[UO_2L(H_2O)(OAc)].H_2O	3430 r	3392, 3252	1665	1551	____	511	469	918 (U=O) 1458$\nu_{as}(COO^-)$, 1217$\nu_s(COO^-)$; (unidentate OAc^-)

instrument mass spectrometer (70 eV). Magnetic susceptibilities of the complexes were measured by the Gouy's method at room temperature using Johnson Matthey, Alfa product, Model No. (MKI), the diamagnetic corrections were calculated from Pascal's constants for all atoms in the compounds [43]. Thermal gravimetric analysis (TGA) of the current compounds were measured from room temperature up to 800 °C (10 °C/min), using a Shimadzu TGA-50H instrument. Melting points were measured in open capillaries on a Stuart SMP3 melting point apparatus.

3. Results and discussion

The Schiff base ligand, HL, and its complexes with Cu(II), Ni(II), Co(II),VO(IV), Zn(II), Cd(II) and UO_2(VI) ions are colored, stable in air and soluble in most common solvent. The elemental analysis, melting points, percentage yields and colors of the free ligand, HL, and its metal complexes are listed in Table 1.

3.1. The Schiff base (HL) ligand

The IR spectral bands and their tentative assignments of the Schiff base ligand, HL, and its metal complexes are given in Table 2. Comparison the IR spectrum of the current Schiff base ligand with that of 5-acetyl-4-hydroxy-2*H*-1,3-thiazine-2,6(3*H*)-dione (AHTD) and *o*-phenylenediamine, was important to confirm the condensation reaction *via* the IR absorption bands. Consequently, the appearance of an intense band at 1622 cm^{-1} that assigned to the azomethine ν(C=N) band and disappearance of the absorption band at 1659 cm^{-1} of the acetyl C=O of AHTD, that condensed with the NH_2 group of the *o*-phenylenediamine confirmed the structure of the ligand as suggested in Scheme 1. The IR spectrum of the free ligand also revealed characteristic absorption bands at 3463, (3388, 3315), 3222, 1661, 1622 and 1544 cm^{-1} those assignable to OH, NH_2, NH, 2C = O, C=N and C=C functional groups, respectively [44,45].

The mass spectrum of the Schiff base (HL) showed the molecular ion peak at m/e = 277 confirming the molecular formula $C_{12}H_{11}N_3O_3S$ corresponding to the formula mass (277.30 amu). The fragmentation pattern of the mass spectrum is described in Scheme 2.

The ^{1}H NMR spectrum (Fig. 1) of the current HL ligand showed characteristic singlet signal at δ 2.37 ppm which might attribute to the methyl protons, in addition to broad exchangeable signals at δ 5.37 (NH_2), 12.00 ($NH_{thiazine}$) and 13.60 ppm ($OH_{thiazine}$) as illustrated in Table 3. Also, the ^{13}C NMR spectrum (Fig. 2, Table 4) of the ligand showed eleven signals which are ascertained to the number of carbon atoms in HL ligand. Moreover, characteristic signal appeared in the upfield region at δ 15.8 ppm assignable to CH_3 carbon.

Electronic spectral data of the free ligand in DMF solution showed absorption bands at 276 and 300, 338nm like those reported for similar Schiff base compounds [30,46]. The higher energy band could be assigned to the π → π* transition of the azomethine group, and the lower energy bands may be assigned to the *n* → π* transitions resulting from nitrogen, and oxygen [47].

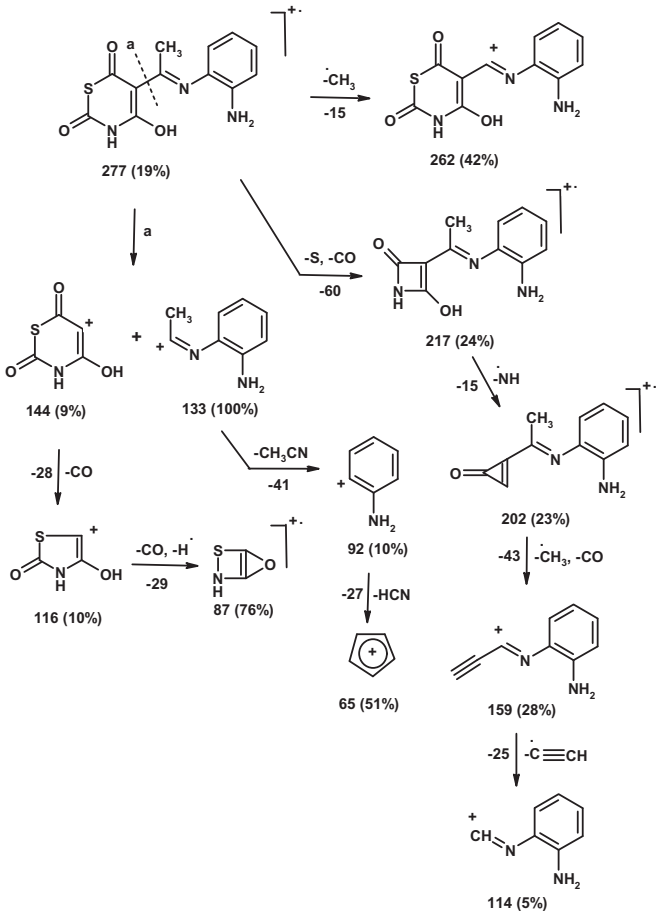

Scheme 2. Mass fragmentation patterns of the ligand.

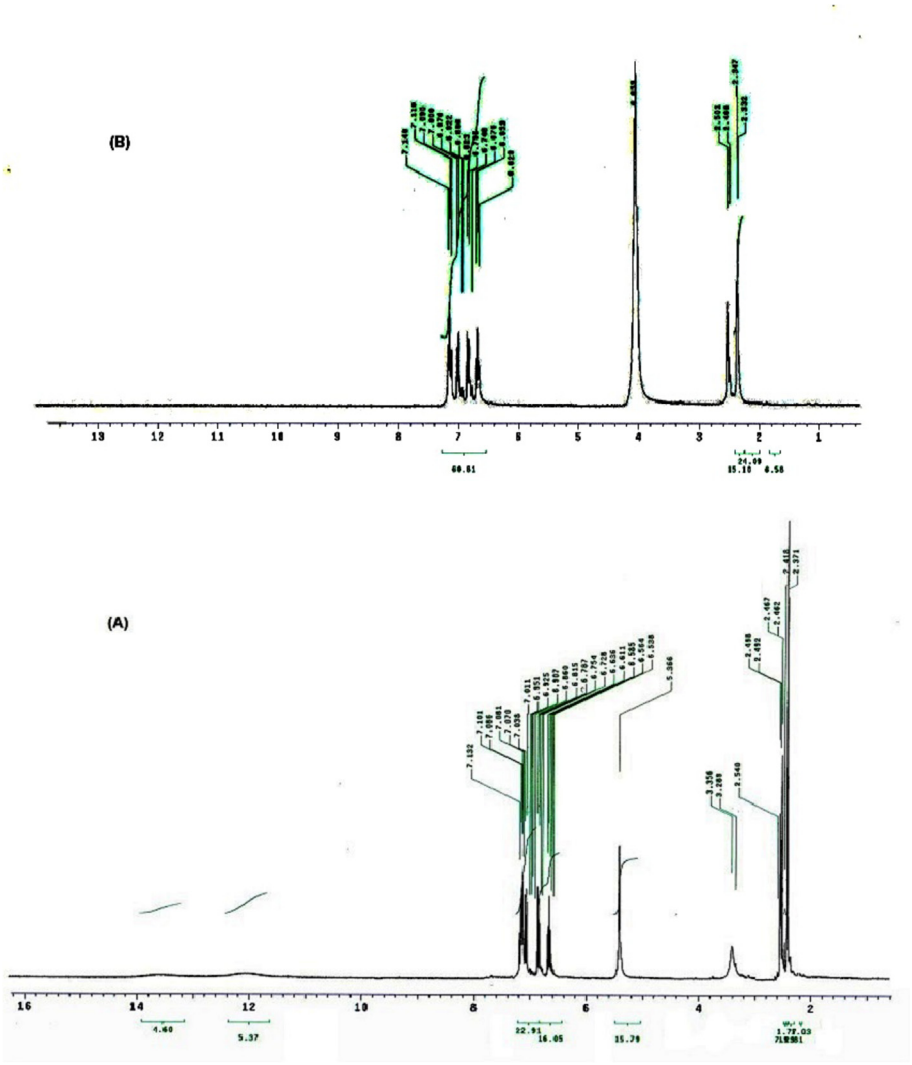

Fig. 1. ^{1}H NMR spectra (δ, ppm) in DMSO-d_6 solvent of: (**A**) HL ligand without addition of D_2O and (**B**) HL ligand after the addition of D_2O.

Table 3
^{1}H NMR spectra of the, HL, ligand and its and complexes.

^{1}H NMR Chemical shifts in ppm			
HL ligand	Cd(II) Complex(**6**)	UO_2(IV) complex (**7**)	Assignment
2.37	2.36	2.33	(s, 3H, CH_3) (s, 2H, NH_2 exchangeable with D_2O)
5.37	5.28	5.28	(t, 1H, $J = 7.8$ Hz,Ar–H)
6.56	6.55	6.57	(d, 1H, $J = 8.4$ Hz,Ar–H)
6.79	6.72	6.73	(d, 1H, $J = 8.1$ Hz,Ar–H)
7.02	6.93	6.89	(t, 1H, $J = 7.8$ Hz,Ar–H)
7.11	7.09	7.09	(brs,1H, NH exchangeable with D_2O)
12.00	11.07	–	(brs,1H, OH exchangeable with D_2O)
13.60			

3.2. Metal complexes

The Schiff base ligand was allowed to react with Cu(II), Ni(II), Co(II), Zn(II), Cd(II), VO(IV) and UO_2(VI) ions to yield the corresponding metal complexes. The isolated complexes were characterized by elemental analysis, FT-IR, UV–Visible, mass, ESR, ^{1}H NMR spectroscopy and thermal gravimetric analysis (TGA), as well as molar conductance and magnetic susceptibility measurements. All the metal complexes have 1:1 (metal: ligand) stoichiometry except Ni(II)-,VO(VI) complexes which have 1:2 (metal: ligand) stoichiometry.

The molar conductance values of the current complexes in DMF (10^{-3}) solutions are shown in Table 5. The present complexes are neutral except complexes **1** and **3** which revealed molar conductance values 86 and 100 $\Omega^{-1}cm^2$/mol, respectively, indicating 1:1 electrolytes, so the NO_3^- anions are in the outer sphere [48].

3.2.1. Infrared spectra

The main characteristic IR vibrational frequencies and their assignments for the current complexes are given in Table 2. The sites

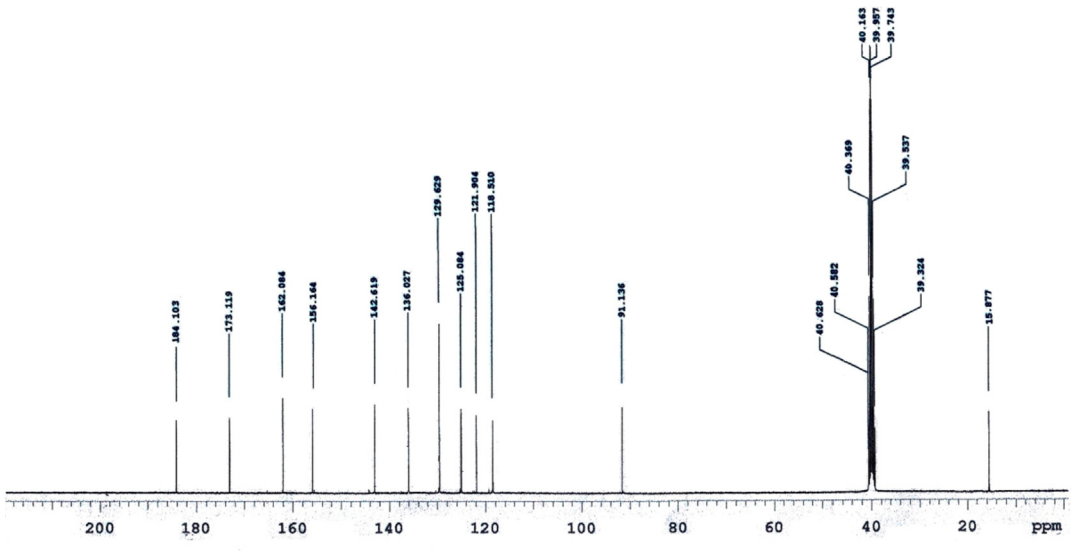

Fig. 2. ^{13}C NMR spectrum of HL ligand.

Table 4
^{13}C NMR spectral data of the Schiff base, HL, ligand.

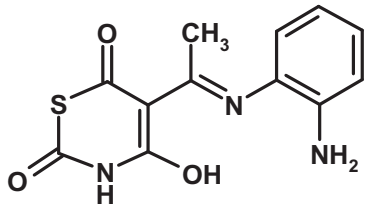

Chemical shifts in ppm (DMSO)	Assignment
15.8	CH_3
91.1	C-5
118.5	Ar–C
121.9	Ar–C
125.0	Ar–C
129.6	Ar–C
136.0	Ar–C
142.6	Ar–C
156.1	C=N
162.0	C=O as C-2
173.1	C=O as C-6
184.1	C-4

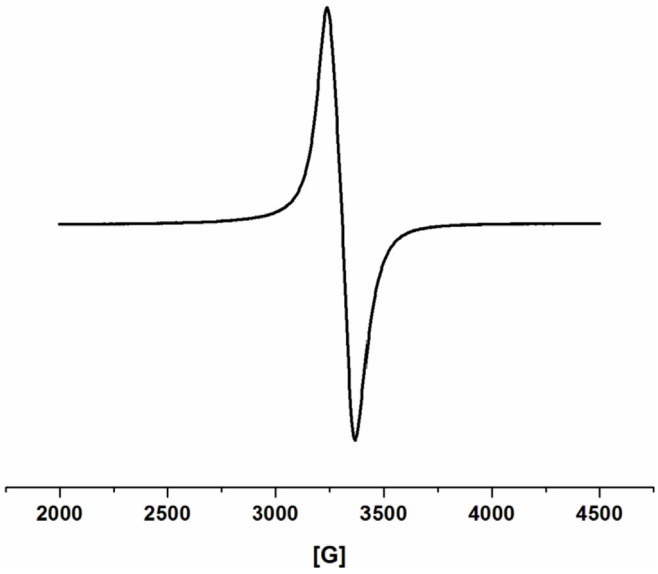

Fig. 3. ESR spectrum of $[CuL(H_2O)]NO_3.0.5H_2O$ **1**.

of coordination were concluded from the comparison of the IR data of the free ligand with its complexes. The shift of ν(C=N) of the free ligand at 1622 cm^{-1} to a lower frequencies by 34–98 cm^{-1} in the complexes indicating coordination through the azomethine nitrogen (C=N) [49]. The broad bands in the range of 3464-3422 cm^{-1} could be assigned to the stretching frequencies of ν(OH) of water and/or methanol molecules, as confirmed by the elemental analysis and thermal analysis.

The coordination modes of the anions could be deduced from the IR spectral bands, complex **7** displayed absorption bands at 1458 and 1217 cm^{-1} those assigned to ν_{as} and ν_s stretching

Table 5
UV–Visible spectral data, molar conductance and magnetic moments of the metal complexes of the HL ligand.

	Ligand/complex	$\pi - \pi^*$	n- π^*	d-d transition bands	Λ Ohm^{-1} cm^2mol^{-1}	μ_{eff}
	HL	276	300, 338	____	____	____
(1)	$[CuL(H_2O)]NO_3.0.5H_2O$	284	307, 350	544	86	1.70
(2)	$[Ni(L)_2].2H_2O$	283	315,352	402,574	12	2.95
(3)	$[CoL(H_2O)_3]NO_3.1.5CH_3OH$	290	303,350	400,542	100	4.82
(4)	$[VO(L)_2].3H_2O$	284	310,353	590	14	1.65
(5)	$[Zn(L)(H_2O)_2NO_3].H_2O$	284	355	____	20	____
(6)	$[CdL(CH_3OH)_2\ NO_3]$	283	356	____	26	____
(7)	$[UO_2L(H_2O)(OAc)].H_2O$	____	313	434, 537	30	____

frequencies of carboxyl group, respectively, suggesting monodentate character of the CH_3COO^- group [50]. Whereas complex **1** exhibited two bands at 1390 and 820 cm^{-1} indicating the presence of ionic nitrate [46]. However, in complexes **5** and **6** the NO_3^- group acts as an unidentate due to the existence of two bands at (1350, 1216 cm^{-1}) and (1356, 1230 cm^{-1}), respectively [51].

Furthermore, the IR spectrum of VO(IV) complex **4** displayed absorption band at 1095 cm^{-1} due to the stretching vibration of the ν(V═O) band in hexa-coordinated structure [52]. Similarly, the strong band located at 918 cm^{-1} for complex **7** was assigned to $\nu_{3(asym)}$ of the O═U═O vibration [53]. The observed values of ν(V═O) and ν_3(O═U═O) are utilized to calculate the force constant (F) of V═O and O═U═O by using McGlynn and Smith relation [54], yielding 9.899 and 6.957, respectively. In addition, Jones relation used to calculate the force constant values which used to calculate the M – O distance [55], which was found to be 1.673 and 1.736 for oxovanadium (IV) and dioxouranium (VI) complexes, respectively. The calculated force constant and M – O distance values are consistent with the normal range for oxovanadium (IV) and dioxouranium(VI) complexes [56].

The frequencies of the weak bands in the range 473-426 cm^{-1} and 560-507 cm^{-1} are attributed to ν(M – O) and ν(M – N), respectively [50].

3.2.2. Electronic spectra and magnetic moment measurements

The electronic spectral bands of the present metal complexes in DMF solution with their tentative assignments along with magnetic moments values are given in Table 5. The bands in the vicinity of free ligand, n→ π* and π→ π* are red-shifted by 7–14 and 12–17 nm, respectively, in the current metal complexes.

The electronic spectrum of Cu(II) complex **1** showed band at 544 nm, that assigned to $d_{xy} \rightarrow d_{x2\text{-}y2}$ ($^2B_1 \leftarrow ^2B_2$), indicating a square planar geometry [30,57]. The magnetic moment value for Cu(II) complex **1** (Table 5) was found in the range reported for d^9 systems containing one unpaired electron (1.70 B M), confirming the square planar geometry of the complex [58].

The electronic spectrum of Ni(II) complex **2** showed two absorption bands at 574 and 402 nm assigned to $^3T_{1g}(F) \leftarrow {}^3A_{2g}(F)$ and $^3T_{1g}(P) \leftarrow {}^3A_{2g}(F)$, respectively, indicating octahedral structure [59]. The magnetic moment value of Ni(II) complex **2** is 2.95 B M., which lies in the range (2.9–3.3 B M) of the Ni(II) octahedral

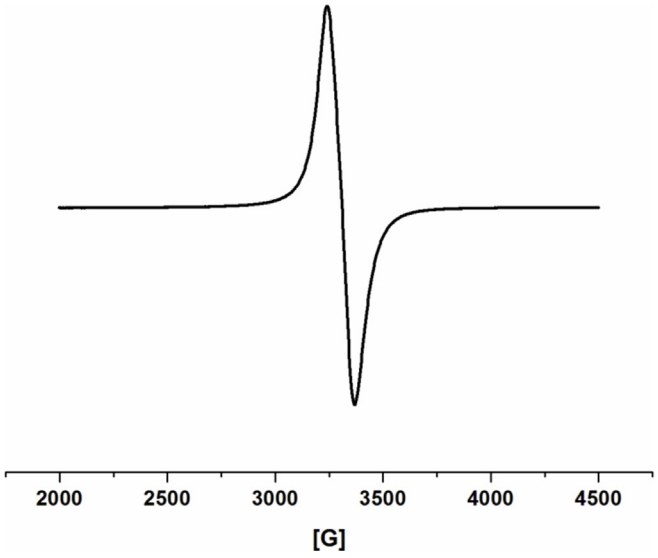

Fig. 4. ESR spectrum of $[VO(L)_2].3H_2O$ **4**.

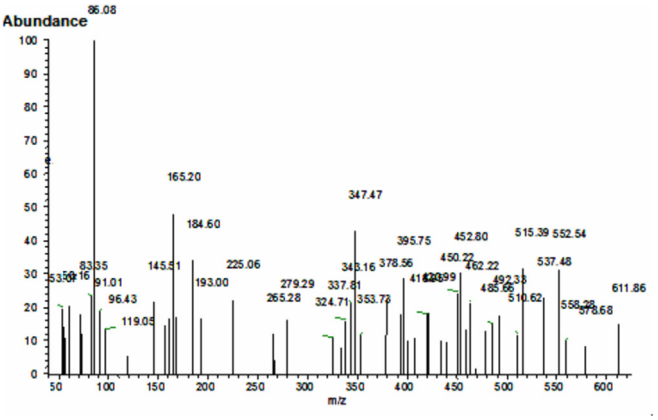

Fig. 5. Mass spectrum of $[Ni(L)_2].2H_2O$ **2**.

complexes [60]. The spectral data provide the ligand field parameters: B (441 cm^{-1}), 10Dq (1233 cm^{-1}) and β (0.41), and predicted the first transition band, $^3T_{2g}(F) \leftarrow {}^3A_{2g}(F)$, at 12,330 cm^{-1}.

The electronic spectrum of Co(II) complex **3** exhibited two bands at 400 and 542 nm, assignable to, $^4T1g(P) \leftarrow {}^4T1g(F)$ and $^4A_{2g}(F) \leftarrow {}^4T_{1g}(F)$ transitions, recommending octahedral geometry [61]. The ligand field parameters were calculated B (366 cm^{-1}), 10Dq (1098 cm^{-1}) and β (0.38); the third band not observed, but it can be calculated and found at 13,725 cm^{-1}, these values found within the range reported for octahedral structure [62]. The magnetic moment value is 4.82 B M., therefore, a high-spin octahedral geometry for the Co(II) complex **3** was proposed [32,63].

The electronic spectrum of the oxovanadium(IV) complex **4** showed band at 590 nm due to $b_1 \leftarrow b_2$ electronic transition, suggesting octahedral structure [63]. The magnetic moment measurement value is $\mu_{eff} = 1.65$ B M.

The Zn(II) **5** and Cd(II) **6** complexes showed two absorption bands at 284, 283 and 355, 356 nm which might attribute to π → π* and n → π* transitions, respectively, in the vicinity of the Schiff base ligand.

The UO_2(VI) complex **7** showed three absorption bands at 313, 434 and 537 nm, which might arise from the allowed electronic transitions of n → π* and metal → ligand charge transfer (MLCT) and/or appical oxygen → F^o (U) [64]. The magnetic moment measurement suggested the diamagnetic geometry of the UO_2(VI) complex as expected [65].

The ^{1}H NMR spectral data of Cd(II) and UO_2(VI) complexes

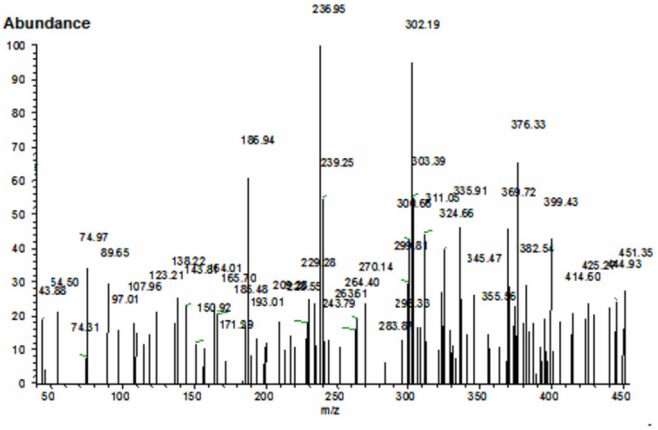

Fig. 6. Mass spectrum of $[CoL(H_2O)_3]NO_3.1.5CH_3OH$ **3**.

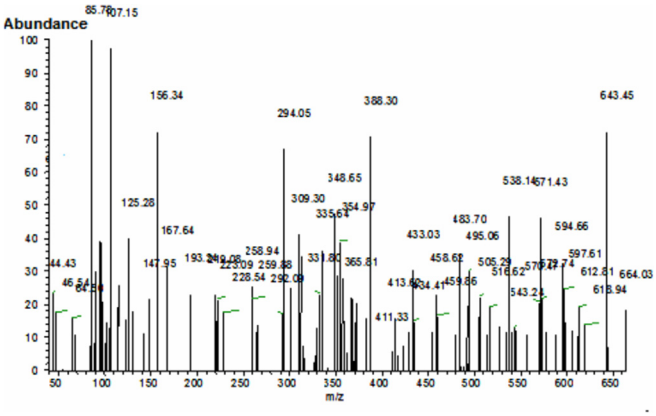

Fig. 7. Mass spectrum of $[VO(L)_2].3H_2O$ **4**.

(Table 3) showed the aromatic protons in the range (6.55–7.09) and (6.57–7.09) ppm, respectively. A characteristic singlet signal appeared at 2.36 and 2.33 ppm, might attributed to the methyl protons, and a broad exchangeable signal appeared at 11.07 ppm might assigned to $NH_{thiazine}$. Vanishing of the broad signal which appeared at 13.60 ppm ($OH_{thiazine}$) in the ^1H NMR spectrum of the free ligand, suggesting that these protons were deprotonated during the coordination of the Schiff base ligand with the Cd(II) ion and UO_2(VI), supporting the monobasic tridentate behavior.

3.2.3. ESR spectra

Figs. 3 and 4 showed the ESR spectra of Cu(II) complex **1** and VO(IV) complex **4**, in solid state at 25 °C. The ESR spectra of Cu(II) complex **1** exhibited one broad band with $g_{eff} = 2.09$, proposing square planar geometry around Cu(II) ion in the complex such as concluded from its UV/Vis spectra [29]. Whereas, oxovanadium(IV) complex **4**, displayed one band at $g_{eff} = 2.09$ indicating an octahedral geometry around VO(IV) ion corroborative with the results obtained from its IR and UV/Vis spectra [66].

3.2.4. Mass spectra

The mass spectra of complexes **2**, **3** and **4** as representative complexes (Figs. 5–7), Complexes **2**, **3** and **4** provide good evidence for the molecular formulas from their highest mass peak at *m/z* 611, 461 and 664 respectively, which agree well with the proposed formula weights for the non-hydrated or non-solvated complexes: $[Ni(L)_2].2H_2O$ (F. Wt = 647.33), $[CoL(H_2O)_3]NO_3.1.5CH_3OH$ (F. Wt = 499.34), $[VO(L)_2].3H_2O$ (F. Wt = 673.5). The mass fragmentation pattern of complex **4** are represented in Scheme 3.

Eventually, on the basis of the spectral data the structures of the metal complexes are showed in Scheme 4.

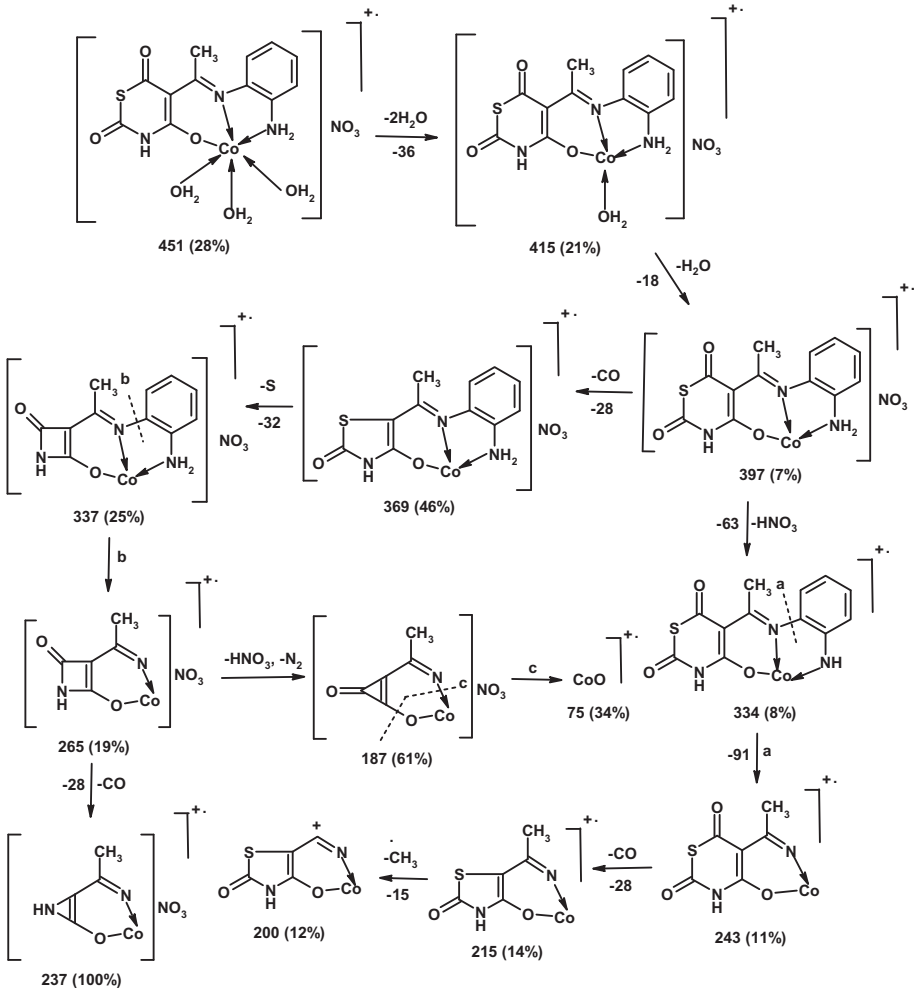

Scheme 3. Mass fragmentation patterns of Co(II)complex.

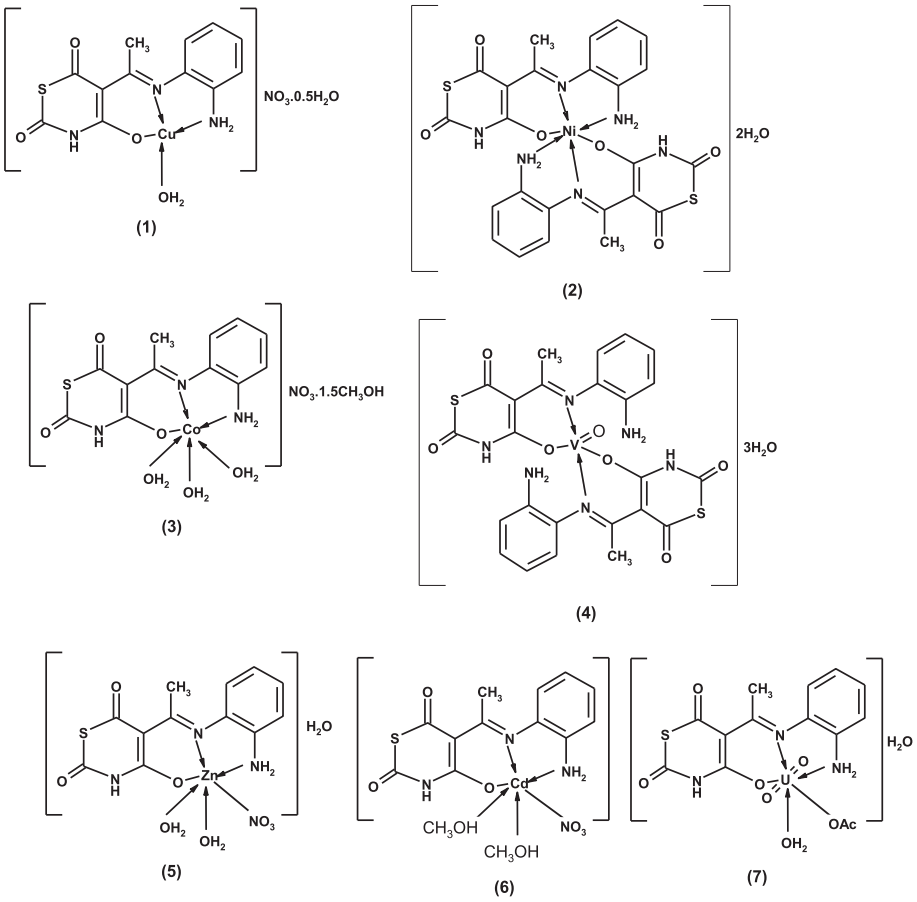

Scheme 4. Representative structures of the metal complexes.

3.2.5. Thermal analysis

Thermal gravimetric analysis was carried out to get information about the thermal stability of the metal complexes and elucidation the presence of water and solvent molecules (if present) in the coordination sphere [67]. Also, thermodynamic parameters using Coats-Redfern equations have been calculated. The results of thermal analysis of the ligand and its metal complexes are summarized in (Table 6). Figs. 8–10 show the representative example for complexes **1**, **3** and **4**.

Complexes **1**–**4** lost the lattice water or methanol molecules at the temperature range (80–120 °C). While, the coordinated water molecules were eliminated from their complexes at higher temperature than those in case of the lattice water molecules. There are two ways in removal of the coordinated water molecules of the complexes. In complexes **3** and **7** which lose only all the coordinated water molecules in the temperature range (113–250 °C). However, in complexes **1** and **6** the elimination of the coordinated water molecules was accompanied with the loss of a part of ligand. HNO_3 molecule loosed from complexes **1**, **3** and **6** at 465 °C, 403 °C and 398 °C, respectively, while CH_3COOH molecule decomposed at 376 °C in complexes **7**.

The kinetic parameters: activation energy (E_a), enthalpy (ΔH^*), entropy (ΔS^*) and free energy changes (ΔG^*) of the thermal degradation of the complexes are calculated as described elsewhere [33] and summarized in (Table 7). Inspection of these data demonstrates the following remarks:

(i) The decomposition stages of all the metal complexes show a best fit of n = 1 which indicate that the first order decomposition and the correlation coefficients of the plots of the thermal decomposition steps were found to lie in the range 0.98–0.99, showing a good fit with linear function.
(ii) The entropy of activation, ΔS^*, of some decomposition steps gave negative value which indicates that the activated fragments have more ordered structure than the undecomposed ones and the later are slower than the normal [68,69].
(iii) The positive values of activation enthalpy change, ΔH^* indicate that the decomposition stages are endothermic processes.
(iv) The positive value of ΔG^* for all the complexes reveals that all the decomposition steps are non-spontaneous processes [70–72].

4. Antimicrobial activity

The antimicrobial activities of synthesized HL and its metal complexes were screened for antibacterial and antifungal properties by agar diffusion method [37,38] in DMF solvent against different types of bacteria; Gram-positive (*S. aureus*) and Gram negative (*P. vulgaris*). Besides, *C. albicans* for fungus. Some

Table 6
TGA results of the HL ligand and its metal complexes.

Compound	DTG peak (°C)	Temperature range (°C)	Decomposition product lost (formula weight)	Weight loss (%) found (calculated)
HL	161	125–181	-$C_3H_4N_2$	24.42 (24.52)
	230	182–267	-2CO+CS	35.94 (36.06)
	550	267–596	-C_6H_8NO	40.00 (39.66)
[$CuL(H_2O)$]NO_3.0.5H_2O (**1**)	73	32–99	−0.5H_2O	2.51 (2.10)
	233	99–250	-H_2O+CH_3CN+2CO+NH	29.60 (30.31)
	465	434–519	-HNO_3	14.37(14.68)
	714	519–800	-C_6H_6 +S	24.01(25.64)
		Residue	-CuO+C_2H_2N	29.52(27.87)
[$Ni(L)_2$].2H_2O (**2**)	110	65–154	-2H_2O	5.43 (5.56)
	247	221–302	-2CH_3CN+4CO+2NH	34.04 (34.60)
	516	305–765	-$C_{16}H_{14}N_2OS_2$	47.03 (48.81)
		Residue	-NiO	13.5 (11.53)
[$CoL(H_2O)_3$]NO_3.1.5CH_3OH (**3**)	76	31–133	−1.5CH3OH	9.70 (9.61)
	152	134–175	-3H2O	8.8 (10.81)
	204	175–220	-C5H4	14.74 (12.83)
	258	220–304	CH3CN+2CO	18.21(19.42)
	403	304–470	C3H3N +HNO3–(CoO + S+ NH)	24.30(23.24)
		Residue		24.25(24.41)
[$VO(L)_2$].3H_2O (**4**)	80	33–185	−3H_2O	8.00 (8.03)
	232	185–253	-CH_3CN+NH	9.82 (8.32)
	285	253–303	-4CO	16.87 (16.64)
	347	314–434	-C_4H_5N3	14.32 (14.11)
	476	434–520	-$C_{12}H_{10}O$	24.07(25.26)
	647	520–798	-CH_3CN	5.29(6.09)
		Residue	-VO_2+S_2	21.34 (21.82)
[$CdL(CH_3OH)_2NO_3$] (**6**)	190	96–200	-CH_3OH	7.82 (6.22)
	282	212–366	-CH_3OH+CH_3CN+ 2CO	25.72 (25.09)
	398	366–464	-HNO_3	11.47 (12.94)
	561	509–638	-C_2H_3N	8.18 (7.97)
		Residue		
			- CdO S+C_6H_5	446.10
[$UO_2L(H_2O)(OAc)$].H_2O (**7**)	75	26–112	-H_2O	2.80 (2.80)
	131	113–154	-H_2O	2.80 (2.80)
	266	155–332	-$C_3H_6CN_3O_2$	19.97 (19.95)
	376	332–467	-CH_3COOH	9.22 (9.35)
	621	467–797	-C_6H_6	12.21(12.16)
		Residue	-(UO_3 + C_2S)	51.28 (48.33)

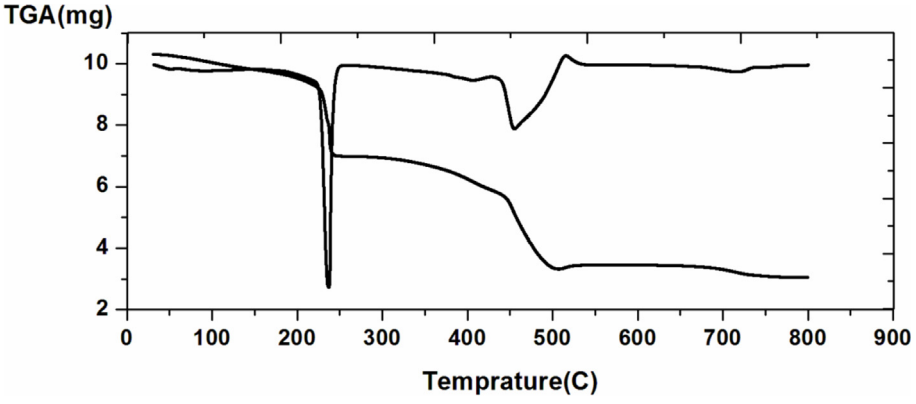

Fig. 8. The TGA-DrTGA curves of complex (**1**).

antibiotics were evaluated for their antibacterial activities and their results were compared with free ligand and its metal complexes.

1) The inhibition effect of the ligand and its metal complexes are presented in Table 8 which revealed that most of the synthesized complexes possess a variety of antimicrobial activities toward all microorganisms, while the ligand showed small indefinite quantity activity toward all types of microorganism
(2) VO(IV) complex **4** showed an excellent activity toward *P. vulgaris* as Gram negative bacteria, while Cu(II) complex **1** showed excellent activity toward *C. albicans* as fungal strain
(3) Cu(II) complex **1** and Ni(II) complex **2** showed an excellent activity toward *S. aureus* as Gram positive bacteria.

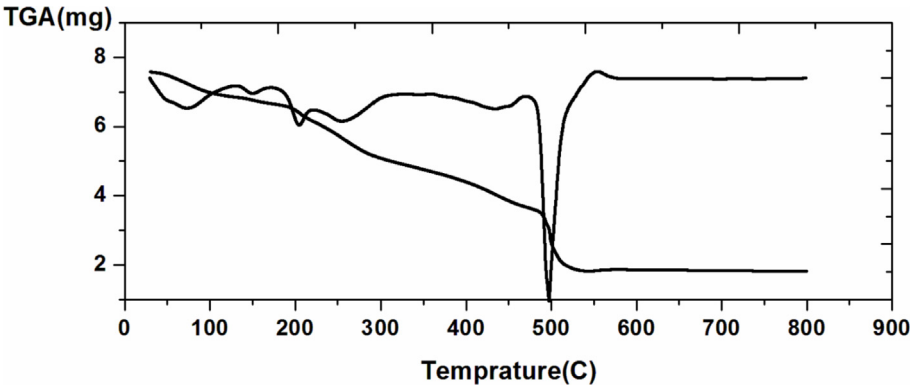

Fig. 9. The TGA-DrTGA curves of complex (**3**).

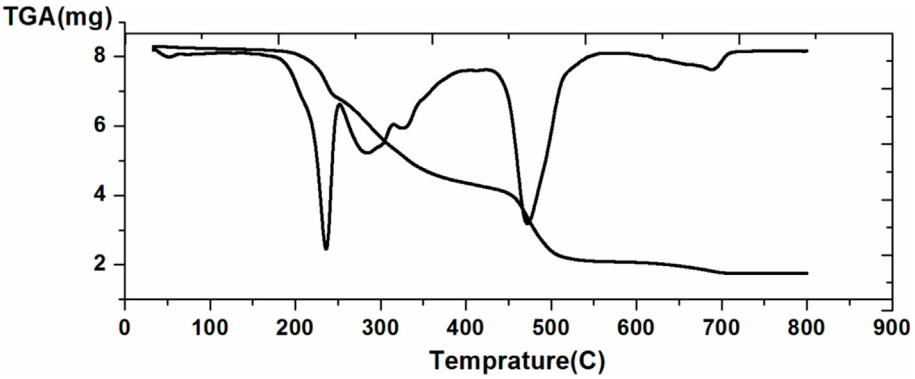

Fig. 10. The TGA-DrTGA curves of complex (**4**).

Table 7
Temperatures of decomposition and the kinetic parameters of HL ligand and its metal complexes.

Compound	Step	n order	T (K)	A (S^{-1})	Δ E (kJ mol^{-1})	ΔH (kJ mol^{-1})	ΔS (kJ $mol^{1}K^{-1}$)	ΔG (kJ mol^{-1})
HL	First	1	434	2.3×10^6	32.56	28.95	−0.134	87.11
	Second	1	503	5.8×10^7	83.25	77.40	−0.108	132.20
	third	1	823	6.32×10^8	88.32	81.39	−0.093	157.93
$[CuL(H_2O)]NO_3.0.5H_2O$ (**1**)	First	1	346	8.3×10^6	29.68	26.81	−0.113	65.91
	Second	1	506	2.3×10^6	38.75	34.54	−0.135	102.85
	Third	1	660	7.4×10^7	27.35	22.86	−0.109	94.80
	Fourth	1	737	3.4×10^5	85.88	79.75	−0.154	193.25
$[Ni(L)_2].2H_2O$ (**2**)	First	1	383	2.33×10^5	33.54	30.36	−0.152	88.57
	Second	1	520	4.5×10^7	36.85	32.53	−0.11	89.73
	Third	1	789	2.7×10^{10}	80.35	73.79	−0.062	122.71
$[CoL(H_2O)_3]$ $NO_3.1.5CH_3OH$ (**3**)	First	1	349	4.5×10^5	34.80	31.89	−0.146	82.84
	Second	1	425	6.1×10^9	9.05	5.51	−0.068	34.41
	Third	1	477	2.7×10^{10}	89.54	85.57	−0.0.57	112.76
	Fourth	1	531	2.4×10^8	22.03	17.62	−0.097	69.13
	Fifth	1	676	5.9×10^9	20.12	14.49	−0.073	63.83
$[VO(L)_2].3H_2O$ (**4**)	First	1	353	9.9×10^6	26.39	23.45	−0.121	66.16
	Second	1	505	1.2×10^9	23.69	19.49	−0.083	61.41
	Third	1	558	1.3×10^9	23.69	19.05	−0.080	63.69
	Fourth	1	620	1.9×10^{10}	17.02	11.86	−0.062	50.30
	Fifth	1	749	1.9×10^7	98.11	91.88	−0.121	182.51
	Six	1	920	6.3×10^7	74.41	74.41	−0.11	167.96
$[UO_2L(H_2O)(OAc)].H_2O$ (7)	First	1	348	1.37×10^7	45.39	42.49	−0.117	83.21
	Second	1	404	8.2×10^5	36.92	33.56	−0.143	91.33
$[CdL(CH_3OH)_2NO_3]$ (6)	First	1	463	2.8×10^6	33.54	29.69	−0.133	91.27
	Second	1	555	3.8×10^6	42.36	37.75	−0.132	111.01
	Third	1	671	5.5×10^6	76.00	70.42	−0.131	158.32
	Fourth							
	1	834	6.22×10^7	43.52	36.59	−0.112	130.48	

Table 8
The antimicrobial activity of the HL ligand and its metal complexes.

	Compound	Diameter of inhibition zone (mm) conc. (100 μg mL^{-1})		
		C. albicans (Fungal strain)	*P. vulgaris* (Gram -ve)	*S.aureus* (Gram +ve)
HL		___	___	___
(**1**)	$[CuL(H_2O)]NO_3.0.5H_2O$	18	9	16
(**2**)	$[Ni(L)_2].2H_2O$	3	5	15
(**3**)	$[CoL(H_2O)_3]NO_3.1.5CH_3OH$	5	–	–
(**4**)	$[VO(L)_2].3H_2O$	14	10	8
(**5**)	$[Zn(L)(H_2O)_2NO_3].H_2O$	10	6	5
(**6**)	$[CdL(CH_3OH)_2\ NO_3]$	–	5	–
(**7**)	$[UO_2L(H_2O)(OAc)].\ H_2O$	5	8	–
	Doxymycin	___	10	15
	Fluconazole	16	___	___

Table 9
Antitumor activity of HL ligand and its Cu(II) and VO(IV) complexes against HepG2 cell line.

Compound	IC $_{50}$ (μg/ml)
HL	244
$[CuL(H_2O)]NO_3.0.5H_2O$ (**1**)	120
$[VO(L)_2].3H_2O$ (**4**)	100
Cisplatin	3.67

IC $_{50}$ = inhibition concentration 50%.

The results indicate that most complexes exhibited higher activity than the free ligand, this is explained on basis of overton's concept and chelation theory [73]. According to overton's concept of cell permeability, the lipid membrance surrounding the cell favors the passage of only lipid soluble materials due to which liposolubility is an important factor which controls the antifungal activity. On chelation, when metal ion chelates with ligand, its polarity will be reduced to a greater extent due to the overlap of the ligand orbital and the partial sharing of positive charge of the metal ion with donor groups. Furthermore, it increases the delocalization of π-electrons over the whole chelate ring, which results in an increase in the lipophilicity of metal complexes. This increased of lipophilicity enhances the penetration of complexes into lipid membrane and restricts further multiplicity of microorganisms. These metal complexes also affect the respiration process of the cell; hence, they block the synthesis of "proteins" which restrict further growth of the organism.

5. Antitumor activity

The results of antitumor activity of the ligand, Cu(II) and VO(IV) complexes against HepG-2 cell lines are listed in Table 9. The result showed that complexes of Cu(II) and VO(IV) are proactive than the free ligand, indicating increase of the antitumor activity upon the coordination. The order of antitumor activity is VO(IV) > Cu(II) > HL, as a conclusion, the Cu(II) and VO(IV) complexes showed the highest activity with promising IC_{50} value (120 and 100 μg mL^{-1}) against HepG-2, which is comparable to that of the standard reference; Cisplatin (Table 9). The difference in anticancer activity between the ligand and the metal complexes may be due to the positive charge of the metal increasing the acidity of ligand function group to bear protons. This leads to stronger hydrogen bonds which enhanced the biological activity [74].

6. Molecular orbital calculations

The molecular structures were proposed on the basis of the spectral, molar conductance, magnetic susceptibility and TGA data which indicated that the prepared complexes were of octahedral and square planar conformations. The design of new molecular

Table 10
Total energy (au), energy of HOMO (ev), LUMO (ev), energy gap (ev), Electronegativity(ev), Hardness(ev), Electrophilicity(ev), Softness(eV^{-1}) and dipole moment (Debye) for the ligand and its metal complexes using B3LYP/6-311G(d,p) level.

Compounds	E_T,au	E_{HOMO} (eV)	E_{LUMO} (eV)	E_{gap} (eV)	Electronegativity χ (ev)	Hardness η(eV)	Electrophilicity ω(eV)	Softness S(eV^{-1})	μ,Ɗ
HL	−1251.9720	−5.8194	−2.3029	3.5165	4.0612	1.7583	8.2467	0.2844	3.5077
1	−2968.6652	−4.5919	−1.3568	3.2351	2.9744	1.6176	4.4235	0.3091	11.5540
2	−4011.7567	−6.0438	−2.4694	3.5744	4.2566	1.7872	9.0593	0.2798	6.3082
3	−2863.8694	−4.3193	−1.7889	2.5304	3.0541	1.2652	4.6638	0.3952	9.1827
4	−3523.3424	−6.1149	−2.9179	3.1970	4.5164	1.5985	10.1989	0.3128	6.1825
5	−3464.4125	−6.4336	−1.9843	4.4493	4.2089	2.2247	8.8574	0.2470	13.2852

Table 11
The selected bond lengths and net charges on metals and active centers of HL ligand and its metal complexes using B3LYP/6-311G(d,p) level.

Compound	Charges														
	O15	O16	O17	NH	-C=N	NH_2	S	M	C=O15	C=O16	C–O17	M-O17	-C=N-M	M-NH_2	V=O
HL	−0.384	−0.359	−0.597	−0.713	−0.306	−0.905	0.298	–	1.2361	1.2281	1.3663	–	–	–	–
1	−0.344	−0.342	−0.611	−0.410	0.557	0.695	0.119	0.835	1.2144	1.2058	1.2680	1.9512	1.0907	1.9825	
2	−0.307	−0.257	−0.547	−0.486	−0.634	0.617	0.480	1.307	1.2167	1.2065	1.2376	1.5205	1.9461	1.9773	
	−0.347	−0.265	−0.423	−0.466	−0.737	0.557	0,398		1.2095	1.2052	1.8423	1.8423	1.9090	3.1116	
3	−0.332	−0.334	−0.613	−0.428	0.644	0.617	0.132	0.600	1.2116	1.2071	1.2778	1.8590	1.8610	1.9561	
4	−0.341	−0.357	−0.554	−0.412	−0.431	0.601	0.114	V(1.44)	1.20,007	1.3451	1.3158	1,9274	2.1162	–	1.5760
	−0.294	−0.315	−0.425	−0.334	−0.637	0.662	0.193	O(-0.48)	1.2118	1.2136	1.2575	1.9400	2.4400	–	
5	−0.337	−0.320	−0.605	−0.404	−0.695	0.660	0.138	0.546	1.2135	1.2055	1.2657	1.0235	1.0924	2.2339	

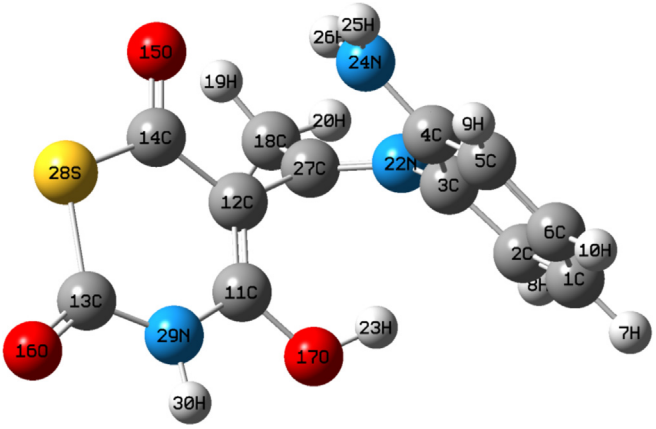

Fig. 11. The optimized structure and numbering system of HL ligand.

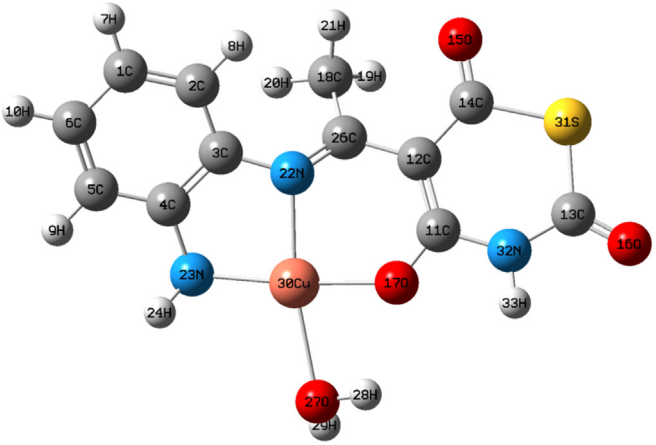

Fig. 13. The optimized structure and numbering system of the Cu(II) complex (**1**).

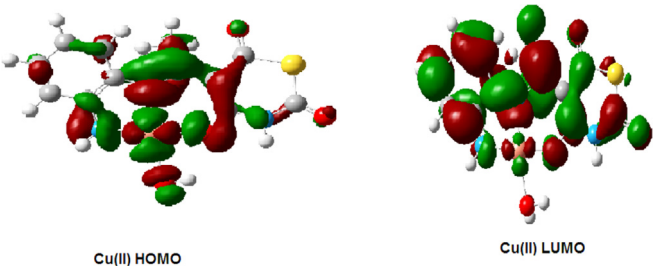

Fig. 14. HOMO and LUMO of the Cu(II) complex **(1)**.

Schiff base ligand and its metal complexes can be recognized by applying computational chemistry tools, which is an effective protocol for interpreting their stabilities and calculating structural parameters (Tables 10 and 11). The structural parameters of the ligand and its metal complexes were performed using density functional theory (DFT) at B3LYP/6-311G (pd) level by the Gaussian 09 program in the gas phase [36]. The visualization of the results/optimized geometries was accomplished by using Gauss View 05. The values of quantum chemical such as, dipole moment and frontier molecular orbitals (FMO), highest occupied and lowest unoccupied molecular orbitals energies, (HOMO, LUMO) are collected in (Table 10). Figs. 11–14 represent numbering system, net charge, the vector of dipole moment, HOMO and LUMO of the ligand and its Cu(II) complex. It is well established that HOMO orbitals are directly related to the ionization potential (electrondonating), whereas LUMO orbitals are directly related to the electron affinity. The molecular hardness and softness of a compound can be predicted from the HOMO-LUMO gap [74]. Hard molecules have a large energy gap and soft molecules have a small energy gap [75,76]. The lowering in the HOMO and LUMO energy gap explains the eventual charge transfer interactions that take place within the molecule.

Figs 11–14 represent the Frontier Molecular Orbital (FMO) analysis that showed the HOMO is mainly concentrated on the oxygen (keto groups, OH phenolic), azomethine nitrogen (-C=N-) and nitrogen amino group (NH_2). However, the LUMO is mainly concentrated on the phenyl ring and hetero ring moiety indicating that the HOMO-LUMO are mostly the p-*anti*-bonding type orbitals. The FMO energy parameters such as the E_{HOMO}, E_{LUMO}, and E_{gap} are often used as reactivity or stability structures [77]. The order of E_{gap}(eV) that measures the reactivity of the current compounds is: Zn(II) > Ni(II) > HL > Cu(II) > VO(II) > Co(II), as shown in Fig. 15. The studied antitumor reactivity mentioned above for HL,VO(IV) and Cu(II) compounds against Erlish Ascites Carcinoma cell line, is nearly agree with the decreasing of the calculated E_{gap} values (Tables 8 and 9). Therefore, the order of antitumor reactivity is VO(II)>Cu(II)>HL complex.

Moreover, the biological activity of the investigated compounds increases with the increasing of the theoretically computed HOMO energies (see section antimicrobial activity) as represented in Figs. 16 and 17 that showed the relation between E_{HOMO} of the current compounds against their activity toward *C. albicasn* (Fungal strain) and *S. aureus* (Gram+Ve).

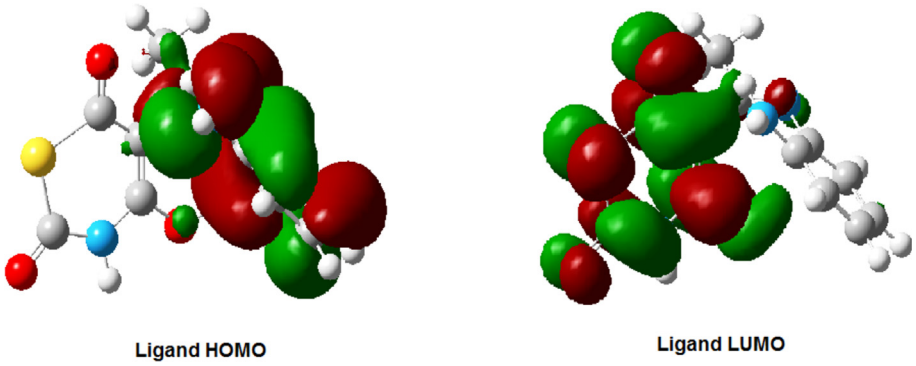

Fig. 12. HOMO and LUMO of HL ligand.

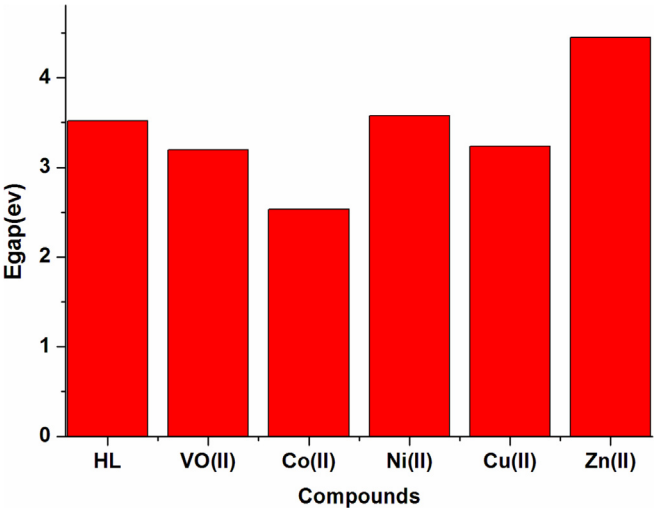

Fig. 15. E_{gap} of the ligand and its metal complexes.

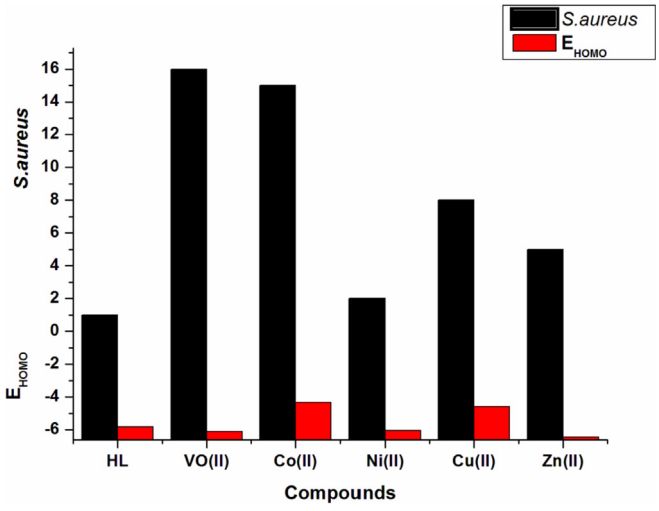

Fig. 17. Relation between E_{HOMO} of the ligand and its metal complexes and their. reactivity toward *S. aureus* (Gram+Ve).

7. Conclusion

A novel tridentate N_2O Schiff base ligand derived from 5-acetyl-4-hydroxy-2*H*-1,3-thiazine-2,6(3*H*)-dione and *o*-phenlenediamine has been synthesized. Metal complexes of Cu(II), Ni(II), Co(II), Zn(II), Cd(II), VO(IV) and UO_2(VI) have been synthesized. The structures of the complexes were proposed based on elemental analyses, spectral data, magnetic moment, molar conductance and thermal complexes showed antimicrobial activity against the microorganisms *S. aureus* and *P. vulgaris* and *C. albicans* for fungus. The ligand and its Cu(II) and VO(IV) complexes exhibited antitumor activity against Human Hepatocelluar Carcinoma. Molecular parameters of the ligand and its metal complexes have been calculated and correlated with the experimental data. Kinetic parameters of the thermal decomposition stages of the ligand and its metal complex

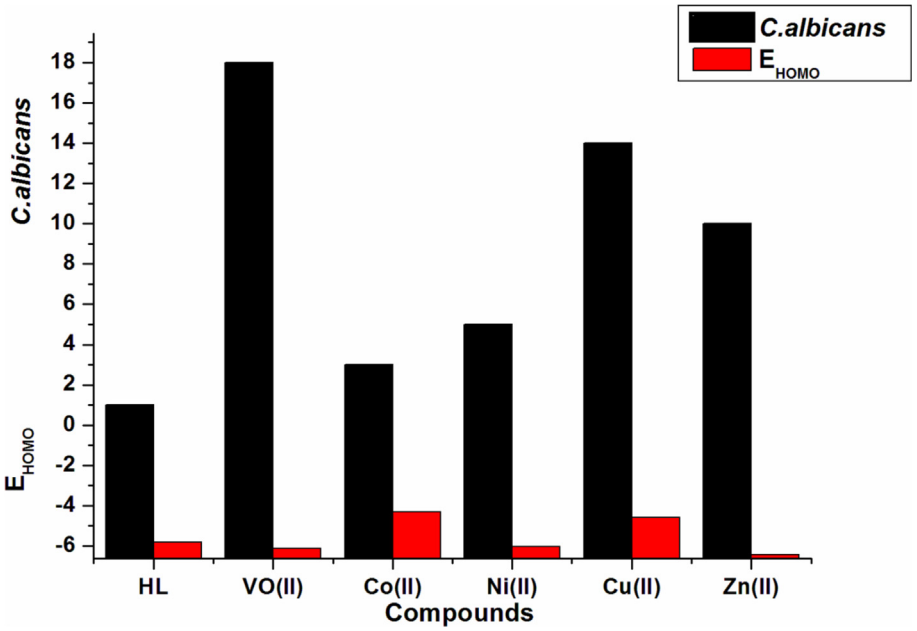

Fig. 16. Relation between E_{HOMO} of the ligand and its metal complexes and their. reactivity toward *C. albicans* (Fungal strain).

gravimetric analysis. Square planar and octahedral geometries have been assigned to the prepared complexes, while uranium(VI) ion is hepta-coordinated in its complex. The ligand and its metal have been evaluated using Coats-Redfern equations. Density Functional Theory calculations were carried out to investigate the optimized structures of the ligand and its metal complexes.

References

[1] A.H. Kianfar, H. Farrokhpour, P. Dehghani, H.R. Khavasi, Spectrochim. Acta A. 150 (2015) 220.
[2] H. Sun, J. Zhang, Y. Cai, W. Liu, X. Zhang, Y. Dong, Y. Li, Polyhedron 125 (2017) 135.
[3] N. Jin, J. Coord. Chem. 65 (2012) 4013.
[4] D.N. Dhar, C.L. Taploo, J. Sci. Ind. Res. 41 (1982) 501.
[5] S. Ghosh, Nayan Roy, T.S. Singh, N. Chattopadhyay, Spectrochim. Acta, Part A 188 (2018) 252.
[6] B. Gao, D. Zhang, Y. Li, Opt. Mater. 77 (2018) 77.
[7] R. Yerrasani, M. Karunakar, R. Dubey, A.K. Singh, T.R. Rao, J. Mol. Liquids. 248 (2017) 214.
[8] A. Taha, A.A.M. Farag, O.M.I. Adly, N. Roushdy, M. Shebl, H.M. Ahmed, J. Mol. Struct. 1142 (2017) 66.
[9] A. Taha, A.A.M. Farag, O.M.I. Adly, N. Roushdy, M. Shebl, H.M. Ahmed, J. Mol. Struct. 1139 (2017) 31.
[10] H. Chang, L. Jia, J. Xu, Z. Xu, R. Chen, W. Wu, H. Bie, T. Zhu, T. Ma, Y. Wang, Inorg. Chem. Commun. 57 (2015) 8.
[11] Y. Harinath, D.H.K. Reddy, B.N. Kumar, Ch Apparao, K. Seshaiah, Spectrochim. Acta A. 101 (2013) 264.
[12] M. Ariyaeifar, H.A. Rudbari, M. Sahihi, Z. Kazemi, A.A. Kajani, H.Z.-B., N. Kordestani, G. Bruno, S. Gharaghani, J. Mol. Struct. 1161 (2018) 497.
[13] K. Poonia, S. Siddiqui, M. Arshad, D. Kumar Neelima, Spectrochim. Acta A. 155 (2016) 146.
[14] A.A. Faheim, S.N. Abdou, Z.H. Abd El-Wahab, Spectrochim. Acta A. 105 (2013) 109.
[15] V.P. Radha, S. Jone Kirubavathy, S. Chitra, J. Mol. Struct. 1165 (2018) 246.
[16] A. Kareem, M.S. Khan, S.A.A. Nami, S.A. Bhat, A.U. Mirza, N. Nishat, J. Mol. Struct. 1167 (2018) 261.
[17] F. Zhao, W. Wang, W. Lu, L. Xu, S. Yang, X.-M. Cai, M. Zhou, M. Lei, M. Ma, H.-J. Xu, F. Cao, Eur. J. Med. Chem. 146 (2018) 451.
[18] B. Iftikhar, K. Javed, M.S.U. Khan, Z. Akhter, B. Mirza, V. Mckee, J. Mol. Struct. 1155 (2018) 337.
[19] M.S. Alam, J.H. Choi, D.U. Lee, Bioorg. Med. Chem. 20 (2012) 4103.
[20] K.S. Kumar, S. Ganguly, R. Veerasamy, E. De Clercq, Eur. J. Med. Chem. 45 (2010) 5474.
[21] S.B. Desai, P.B. Desai, K.R. Desai, Heterocycl. Commun. 7 (2001) 83.
[22] S. Sarkar, S.K. Nag, A.P. Chattopadhyay, K. Dey, Sk M. Islam, A. Sarkar, S. Sarkar, J. Mol. Struct. 1160 (2018) 9.
[23] M.A. Ayoub, E.H. Abd-Elnasser, M.A. Ahmed, M.G. Rizk, J. Mol. Str. 1163 (2018) 379.
[24] R.N. Egekenze, Y. Gultneh, R. Butcher, Inorg. Chim. Acta 478 (2018) 232.
[25] M.S. Behalo, J. Heterocycl. Chem. 55 (2018) 1391.
[26] M. Koketsu, K. Tanaka, Y. Takenaka, C.D. Kwong, H. Ishihara, Eur. J. Pharm. Sci. 15 (2002) 307.
[27] A. Sharma, S. Gudala, S.R. Ambati, S. Penta, Y. Bomma, V.R. Janapala, A. Jha, A. Kumar, J. Chin. Chem. Soc. 65 (2018) 810.
[28] R.A. Haggam, M.G. Assy, M.H. Sherif, M.M. Galahom, Res. Chem. Intermed. 43 (2017) 6299.
[29] O.M.I. Adly, Spectrochim. Acta A. 79 (2011) 1295.
[30] O.M.I. Adly, Spectrochim. Acta A. 95 (2012) 483.
[31] O.M.I. Adly, A. Taha, S.A. Fahmy, J. Mol. Struct. 1054–1055 (2013) 239.
[32] O.M.I. Adly, A. Taha, S.A. Fahmy, J. Mol. Struct. 1083 (2015) 450.
[33] O.M.I. Adly, A. Taha, S.A. Fahmy, J. Mol. Struct. 1093 (2015) 228.
[34] S. Abdel Halim, O.M.I. Adly, Appl. Organomet. Chem. 32 (2018) 1.
[35] V.N. Yuskovets, A.V. Moskvin, B.A. Ivin, Russ. J. Gen. Chem. 74 (2004) 312.
[36] M.J. Frisch, G.W. Trucks, H.B. Schlegel, G.E. Scuseria, M.A. Robb, et al., Gaussian 09. Revision A. 1, Gaussian Inc., Wallingford, CT, USA, 2009.
[37] A.U. Rahman, M.I. Choudhary, W.J. Thomsen, Bioassay Techniques for Drug Development, Harwood Academic Publishers, the Netherlands, 2001.
[38] K.M. Khan, Z.S. Saify, A.K. Zeesha, M. Ahmed, M. Saeed, M. Schick, H.J. Kohlbau, W. Voelter, Arzneim. Forsch. 50 (2000) 915.
[39] T. Mosmann, J. Immunol. Methods 65 (1983) 55.
[40] A.P. Wilson, in: J.R.W. Masters (Ed.), Cytotoxicity and Viability Assay in Animal Cell Culture: A Practical Approach, third ed., Oxford University Press, 2000.
[41] A.I. Vogel, Textbook of "Quantitative Inorganic Analysis, fourth ed., Longman, London, 1978.
[42] T.S. West, Complexometry with EDTA and Related Reagents, third ed., DBH Ltd., Pools, 1969.
[43] F.E. Mabbs, D.J. Machin, Magnitism and Transition Metal Complexes, Dover Publications, New York, 2008.
[44] A.L. El-Ansary, H.M. Abdel-Fattah, N.S. Abdel-Kader, Spectrochim. Acta A. 79 (2011) 522.
[45] M. Amirnasr, F. Fadaee, K. Mereiter, Inorg. Chim. Acta 371 (2011) 6.
[46] M. Shebl, O.M.I. Adly, E.M. Abdelrhman, B.A. El-Shetary, J. Mol. Struct. 1145 (2017) 329.
[47] A.A.A. Emara, A.A. Saleh, O.M.I. Adly, Spectrochim. Acta A. 68 (2007) 592.
[48] W.J. Geary, Coord. Chem. Rev. 7 (1971) 81.
[49] S.M.E. Khalil, A.A.A. Emara, J. Coord. Chem. 55 (2002) 17.
[50] K. Nakamoto, Infrared Spectra of Inorganic and Coordination Compounds, fifth ed., John Willey & Sons, New York, 1997.
[51] M. Shebl, Spectrochim. Acta A. 73 (2009) 313.
[52] T. Rosu, E. Pahontu, C. Maxim, R. Grorgescu, N. Stanica, G.L. Almajan, A. Gulea, Polyhedron 29 (2010) 757.
[53] (a) M. Shebl, Spectrochim. Acta 70 (2008) 850;
(b) M. Shebl, Spectrochim. Acta A. 117 (2014) 127.
[54] S.P. McGlynn, J.K. Smith, W.C. Neely, J. Chem. Phys. 35 (1961) 105.
[55] L.H. Jones, Spectrochim. Acta A. 10 (1958) 395.
[56] H.F. El-Shafiy, M. Shebl, J. Mol. Str. 1156 (2018) 403.
[57] N.N. Greenwood, A. Earnshaw, Chemistry of the Elements, Pergamon Press, NewYork, 1984.
[58] (a) A. Taha, Spectrochim. Acta 59 (2003) 1611.
[59] B.A. El-Sayed, M.M. Abo Aly, A.A.A. Emara, S.M.E. Khalil, Vib. Spectrosc. 30 (2002) 93.
[60] A.A.A. Emara, A.A. Saleh, O.M.I. Adly, Spectrochim. Acta A. 68 (2007) 592.
[61] F.A. Cotton, G. Wilkinson, Advanced Inorganic Chemistry, A Comprehensive Text, fourth ed., John Wiley & Sons, New York, 1986.
[62] J.C. Bailar, H.J. Emeleus, R. Nyholm, A.F. Trotman-Dickenson, Comprehensive Inorganic Chemistry, vol. 3, Pergamon Press, New York, 1975.
[63] A.B.P. Lever, Inorganic Electronic Spectroscopy, second ed., Elsevier, Amsterdam, 1997.
[64] M.C. Saha, R.G. Roy, M.K. Logh, P.S. Roy, Indian J. Chem. 26 (1987) 48.
[65] B. Jezowska, J. Lisowski, A. Vogt, P. Chemielewski, Polyhedron 7 (1988) 337.
[66] N.M. El-Metwally, I. M Gaber, A.A. El-Asmy, A.A. Abou-Hussen, Trans. Met. Chem. 31 (2006) 71.
[67] (a) M. Shebl, O.M.I. Adly, Hoda F. El-Shafiy, S.M.E. Khalil, A. Taha, M.A.N. Mahdi, J. Mol. Struct. 1134 (2017) 649.
[68] S.H. Guzara, Q.H. Jin, Chem. Res. Chin. Univ. 24 (2008) 143.
[69] H.T.S. Britton, Hydrogen Ions, third ed., vol. I, Chapman and Hall, London, 1942.
[70] P.B. Maravalli, T.R. Goudar, Thermochim. Acta 335 (1999) 35.
[71] K.K.M. Yusuff, R. Sreekala, Thermochim. Acta 159 (1990) 357.
[72] S.S. Kandil, G.B. El-Hefnawy, E.A. Baker, Thermochim. Acta 414 (2004) 105.
[73] N. El-wakiel, M. El-keiy, M. Gaber, Spectrochim. Acta A. 147 (2015) 117.
[74] A.S. El-Tabl, M.M. Abd El-Waheed, M.A. Wahba, N.A. Abou El-Fadi, Bioorganic Chem. Appl. (2015) 1, 2015.
[75] K. Dhahagani, S.M. Kumar, G. Chakkaravarthi, K. Anitha, J. Rajesh, A. Ramu, G. Rajagopal, Spectrochim. Acta A. 117 (2014) 87.
[76] H.F. El-Shafiy, J. Mol. Struct. 1166 (2018) 348.
[77] R.G. Pearson, Acc. Chem. Res. 26 (1993) 250.